Journal of Materials Chemistry A

COMMUNICATION

Carbon for oxygen reduction reaction: A defect mechanism†

Huanyu Zhao,‡[ab] Chenghua Sun,‡[c] Zhao Jin,[a] Da-Wei Wang,[d] Xuecheng Yan,[a] Zhigang Chen,[e] Guangshan Zhu[a] and Xiangdong Yao*[af]

We demonstrate a new defect mechanism of carbons for oxygen reduction reaction (ORR). It is predicted by the first principle calculations that a type of 585 defects on graphene (G585) is more effective than N-doping for ORR, and our experimental investigations show strong support to this theoretical prediction.

Oxygen reduction reaction (ORR) is one of the central reactions for fuel cells.[1] To efficiently convert chemical energy to electricity, high performance ORR catalysts become essential. Up to now, platinum (Pt) exhibits the best performance, and Pt/C is the commercial cathode catalyst for fuel cells.[2] It is generally regarded that carbon itself does not show a 4-electron pathway for ORR, and the dispersed Pt particles on carbons are vital and act as the active sites for ORR.[3] However, the high cost and limited supply of Pt have greatly hindered the large-scale application of fuel cells. Therefore, low-cost and high-performance ORR catalysts are indispensable and attracting tremendous interest of research.[4-11] A recent breakthrough is the development of nitrogen-doped carbon and associated structures.[4,12-14] These noble metal-free catalysts could offer good catalytic performance for ORR. It is often believed that N-dopant can activate its neighboring carbon atoms and thus improve oxygen adsorption and dissociation, both of which are critical for ORR.[4,15] Following the N-doping mechanism, extensive efforts have been devoted to achieve highly N-doped carbons, aiming to further enhance their performance.[16-20] However, the electrochemical activity against N concentration shows very diverse (Fig. S1, ESI†). The reasons might be quite complicated, for example, both the N content and the type of N in the carbon samples may influence the performance.[19,20] Another possible reason is the decrement of the electronic conductivity due to heavy N-doping. This indicates that the electrochemical activity cannot be precisely controlled by N-doping, which is a key issue for practical applications as the activity must be stable. Therefore, a basic question comes out: are N-dopants really essential for carbon-based ORR catalysts? In other words, any other mechanisms can promote carbons for ORR?

The proposed mechanism for ORR of N-doped carbons is that the N dopant exhibits higher electronegativity than carbon and thus re-shapes the electronic structure of the neighboring carbon atoms. The re-structured electronic distribution of the carbon atoms enable a stronger interaction with the oxygen molecules, accordingly enhance the oxygen molecular adsorption and dissociation.[15] Consequently, it is natural come to the mind that vacancy defects can be generated if N-dopants are removed from carbon pristine, which will introduce unsaturated carbon atoms with dangling bonds. To this end, the vacancy may bring strong impact on the local electronic structures and the atoms around the vacancy are very reactive. For a pure carbon network, it is presumable that removing a carbon atom (form a vacancy) will have greater effect on the electronic structure of surrounding carbon atoms than replacing a carbon atom by N-doping. It is therefore reasonable to hypothesize that the vacancies are more effective than heteroatom-doping for ORR. However, such single-atom vacancy is not stable and prefers to migrate to combine with other defects to form divacancy, as shown in Fig. 1a, which has been widely observed in irradiated graphene.[21,22] In this work, the divacancy (indicated as G585 because this topological defect contains two pentagons and one octagonal) is selected to study its effect on the ORR performance of carbons in terms of energy profile. Perfect monolayer graphene (G) and N-doped graphene (N-G) also applied as the reference for the calculations. Specifically, four elementary reactions based on the mechanism of peroxy intermediates have been considered, namely $O_2 \rightarrow HO_2^* \rightarrow O^* + OH^- \rightarrow HO^* + OH^- \rightarrow 2OH^-$, and the free energy changes have been calculated under the scheme of density functional theory (DFT, more computational settings are described in the Experimental Section, ESI†). Ideally, all elementary steps are homogeneously exothermic, which can be indexed by the calculated Gibbs free energy changes (ΔG, negative value means exothermic reaction). Besides, an ideal catalyst is also introduced as the guideline for comparison.

[a] Queensland Micro- and Nanotechnology Centre, Griffith University, Nathan, Queensland 4111, Australia. E-mail: x.yao@griffith.edu.au
[b] Institute of Theoretical Chemistry, Jilin University, Changchun 130023, China
[c] Department of Chemistry, Monash University, Clayton, Victoria 3800, Australia
[d] School of Chemical Engineering, University of New South Wales, NSW 2052, Australia
[e] School of Mechanical and Mining Engineering, The University of Queensland, Queensland 4072, Australia
[f] School of Natural Sciences, Griffith University, Nathan, Queensland 4111, Australia
† Electronic supplementary information (ESI) available: Experimental details and additional figures as noted in the text. See DOI: 10.1039/x0xx00000x
‡ These two authors contributed equally to this work.
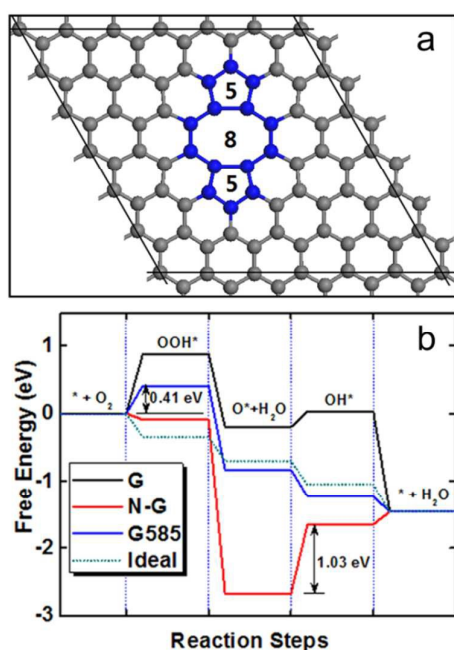
Fig. 1 (a) Pictorial representation of G585 defects in graphene; (b) Calculated free energy diagram of perfect monolayer graphene (G), N-doped graphene (N-G), graphene with G585 defects (G585) and an ideal catalyst (Ideal) for ORR at the equilibrium potentials.

Fig. 2 (a) High-resolution N 1s XPS spectra with deconvolutions, (b) Relative atomic percentage of different nitrogen bonding states, (c) Raman spectra and (d) Histogram of the specific surface area with pore size for the prepared catalysts C-700, 800, 900 and 1000.

As shown in Fig. 1b, N-doped graphene can effectively promote the adsorption of oxygen molecules (O_2) with respect to the perfect sp^2-C network, as indicated by the calculated ΔG for $O_2 \rightarrow OOH^*$ (0.88 eV and -0.09 eV for G and N-G, respectively). However, compared with the ideal catalyst, N-doping is not beneficial for the reduction of chemisorbed oxygen atom (O^*) and high energy input (1.03 eV) is required for the $O^* \rightarrow OH^*$ reaction from our calculations, which is supposed to be the rate-determining step. Similarly, G585 defects can assist the $O_2 \rightarrow OOH^*$ reaction as well, with ΔG reduced from 0.88 eV (on perfect graphene) to 0.41 eV. More importantly, all of the following reactions over G585 are thermodynamically favorable, being close to the ideal catalyst, which is different from N-doping. The calculated results clearly demonstrate that G585 can offer better catalytic performance than N-doping. Previous theoretical calculations revealed that G585 defects can induce dispersive electronic states, but could not produce dangling bonds. Consequently, it is slightly distorted from the ideal sp^2 hybridization with the generation of local strain energy, which can activate local carbon atoms. In addition, G585 defects do not create dangling bonds and they are stable. O-species (O_2, OH, OOH and O) are not strongly bonded over these sites, which accounting for the exothermic of the last three elementary reactions (Fig. 1b). Although only limited defects have been investigated up to now, our study demonstrates that topological defects in the dopant-free carbons may serve as the active sites for ORR.

To experimentally examine the theoretical calculations, a N-enriched porous organic framework material (PAF-40) was used to synthesize the N-doped carbon and the subsequent vacancy defects based carbons. The PAF-40 represents a favorable combination of
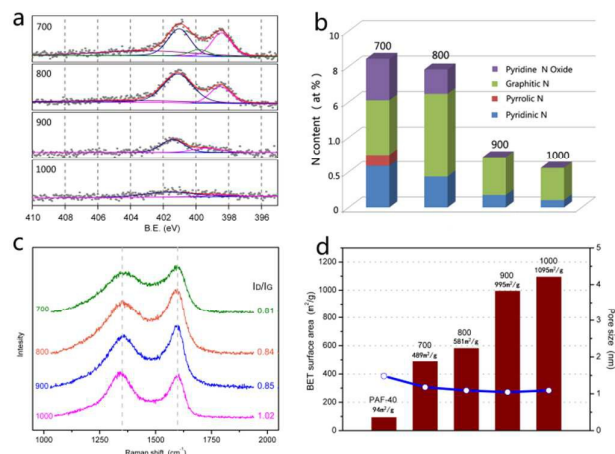
aromatic rings and triazine rings via nitrogen-containing groups (with 12.14 at.% N, see Fig. S2-S6 in ESI† for more details). The periodic arrangement of the construction unit in PAF-40 ensured the uniform distribution of nitrogen. Through heat treatment, PAF-40 is carbonized and at the same time, part of the N-atoms can be released when heated at higher temperatures, leading to the formation of single-atom vacancies. As aforementioned, the single-atom vacancies tend to combine and form divacancies, e.g., G585 defects, which is proved to be stable. Therefore, it is reasonable to hypothesize that the G585 defects are very likely to be formed and other types of defects that are composed of multiple single-atom vacancies may co-exist. In principle, more G585 defects will be produced if more N is removed, so N content can refer to the relative G585 defect density of the carbonized samples.
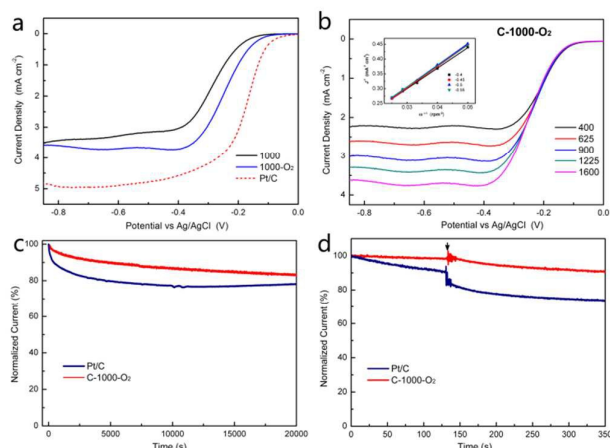
Consequently, we applied a very simple heat treatment process on PAF-40 at 700-1000 °C under nitrogen atmosphere to synthesize a series of partially graphitized carbon samples, denoted as C-700, C-800, C-900, C-1000, respectively. X-ray photoelectron spectroscopy (XPS) was used to examine the N-loss, the N content of the prepared samples (Fig. 2a). It can be seen from Fig. 2b and Table S1 (ESI†) that the N content is monotonically decreased with the increase of the calcination temperature. Table S1 lists the specific values of N content with different N types including pyridinic, pyrrolic, graphitic and pyridine-N-oxide, respectively. Raman spectra (Fig. 2c) indicate that the I_D/I_G ratio increasing from 0.81 to 1.02 monotonically with the carbonization temperature, implying a higher degree of defects of the synthesized samples at higher treating temperatures, which is consistent with the XPS analysis: lower N content (more N lost from PAF-40) reflects more defects. Fig. 2d shows the specific surface area and pore size of the prepared samples versus carbonization temperature. Obviously, the pore size lies in a narrow distribution of ~1.1 nm despite the considerable increase of specific surface areas, suggesting a consistent formation mechanism of the porous structure and the removal of N atoms or the moiety containing N uniformly.
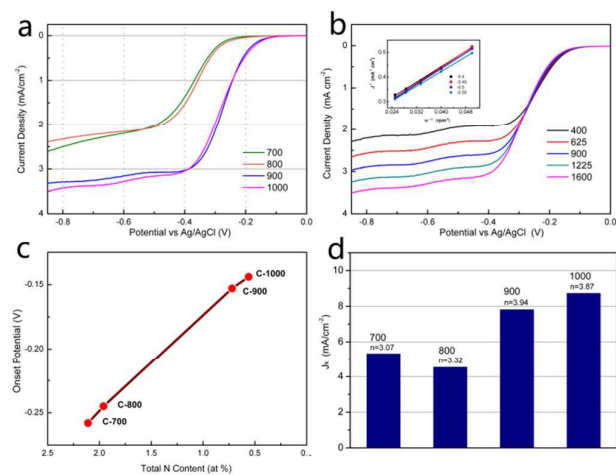
Fig. 3 (a) ORR polarization curves of C-700, C-800, C-900 and C-1000 recorded at room temperature in an O_2-saturated 0.1 M KOH solution with a sweep rate of 10 mV s^{-1} and a rotation rate of 1600 rpm; (b) Rotating-disk voltammogram of C-1000 in O_2-saturated 0.1 M KOH at a sweep rate of 10 mV s^{-1} and different rotation rates (insert: corresponding Koutecky-Levich plot (J^{-1} vs. $\omega^{-0.5}$) at different potentials); (c) onset potentials vs. total N content for catalyst C-700, C-800, C-900 and C-1000; (d) kinetic current densities (J_k) and transferred electronic number based on the Koutecky-Levich plots for C-700, C-800, C-900 and C-1000. The catalyst loading on the RDE for all the samples is 0.12 mg cm^{-2}.

Fig. 4 (a) ORR polarization curves of C-1000, C-1000-O_2 and Pt/C that recorded at room temperature in an O_2-saturated 0.1 M KOH solution with a sweep rate of 10 mV s^{-1} and a rotation rate of 1600 rpm; (b) Rotating-disk voltammogram of C-1000 in O_2-saturated 0.1 M KOH at a sweep rate of 10 mV s^{-1} and different rotation rates (insert: corresponding Koutecky-Levich plot (J^{-1} vs. $\omega^{-0.5}$) at different potentials); (c) i-t chronoamperometric response of C-1000-O_2 and Pt/C in O_2-saturated 0.1 M KOH; (d) CH_3OH-poison effect on the i-t chronoamperometric response for Pt/C and C-1000-O_2. The arrow indicates the addition of CH_3OH into the 0.1 M KOH solution.

The ORR activity of all samples is assessed by cyclic voltammetry (CV) and rotating-disk electrode (RDE) measurements. Samples were loaded onto a glassy carbon electrode and tested in O_2-saturated 0.1 M KOH with Ag/AgCl as the reference electrode. It is clear shown in Fig. 3a that lower N content (more defects) samples exhibit better ORR performance. Both the onset potential (Fig. 3c) and current density (Fig. 3d) are significantly improved with the removal of N, and C-1000 with 0.56 at.% N shows the highest activity among the prepared four samples. LSV curves (Fig. 3a) clearly indicate a one-step pathway for ORR. The electron transfer number for C-900 and C-1000 was calculated to be 3.94 and 3.87, respectively by the Koutecky-Levich plots (Fig. S7 and Fig. 3b), indicating a 4-electron reaction mechanism. For N-doped carbon, it is argued that the type of N directly determine the ORR activity.[12,18] However, in our experiment, it is obvious that the ORR activity is definitely not related to N type. For instance, C-1000 with the highest activity does not contain pyrrolic N or pyridine-N-oxide, and only including a trace of graphitic and pyridinic N (Fig. 2b). This may further indicate that defects are prior to N-dopants for ORR.

To minimize the side effects of different carbonization temperatures on ORR, a control experiment was further carried out under the same conditions of previous C-1000 except introducing a small amount of oxygen to remove more nitrogen. The yielded sample was denoted as C-1000-O_2. As expected, nitrogen in C-1000-O_2 was further removed to only 0.21 at.% (from XPS analysis in Fig. S8, ESI†). Transmission electron microscopy (TEM) images (including selected area electron diffraction), XRD pattern and Raman spectrum of C-1000-O_2 show the typical features of microporous carbon with graphitic layers and significant amount of defects (Fig. S9-S11, ESI†). Unsurprisingly, C-1000-O_2 exhibits superior ORR activity because of the N was further removed. As shown in Fig. 4a, compared to C-1000, the onset and half-wave potentials of C-1000-O_2 are positively shifted by 35 mV and 47 mV, respectively. The current density also slightly increased. Particularly, the ORR activity of C-1000-O_2 is almost comparable to the commercial Pt/C catalyst. For example, the onset potential of C-1000-O_2 is only 43 mV lower than that of Pt/C (Table S1, ESI†). Fig. 4c and d show that C-1000-O_2 demonstrates significantly higher durability and selectivity for ORR with remarkable tolerance to methanol crossover effects (also see Fig. S12, ESI†) than that of Pt/C. The excellent performance of C-1000-O_2 clearly suggests that the defect mechanism proposed in this study is highly effective to promote ORR, and the synthesized carbons are promising substitutions for Pt/C. In this study, we cannot directly observe the G585 defect on the derived carbons due to the high difficulty of such characterization. However, the previous literature reported that the G585 defects could be created and stable on the surface of graphene[23]. This is a strong support that such defects can also be created and existed in the graphitic layers in the synthesized carbons by removing N atoms. Future research on carbons with effective defects but N-free for ORR is desirable.

Conclusions

In summary, a new concept regarding defects can effectively facilitate oxygen reduction reaction is presented. DFT calculations indicate that G585 defects are active and

comparable to Pt in all steps for ORR (close to the ideal catalyst). Meanwhile, the experimental investigations show strong support to the theoretical predictions. The removal of N atoms from carbons could create valuable defects, which contributes to the higher ORR activity. For example, the synthesized carbon with extremely low N content (0.21 at.%) exhibited excellent ORR activity (comparable to Pt/C) and better durability as well as methanol tolerance. Although the produced defects are only characterized by Raman spectroscopy in this study and the proposed defects (G585) have not been observed directly, the newly presented defect mechanism may open a new window to design and fabricate highly efficient ORR catalysts that are possible to replace Pt.

Acknowledgements

Notes and references

1 B. C. H. Steele and A. Heinzel, *Nature*, 2001, **414**, 345–352.
2 R. Borup, J. Meyers, B. Pivovar, Y. S. Kim, R. Mukundan, N. Garland, D. Myers, M. Wilson, F. Garzon and D. Wood, *et al.*, *Chem. Rev.*, 2007, **107**, 3904–3951.
3 R. Bashyam and P. Zelenay, *Nature*, 2006, **443**, 63–66.
4 K. Gong, F. Du, Z. Xia, M. Durstock and L. Dai, *Science*, 2009, **323**, 760–764.
5 M. Lefèvre, E. Proietti, F. Jaouen and J.-P. Dodelet, *Science*, 2009, **324**, 71–74.
6 G. Wu, K. L. More, C. M. Johnston and P. Zelenay, *Science*, 2011, **332**, 443–447.
7 D.-W. Wang and D. Su, *Energy Environ. Sci.*, 2014, **7**, 576–591.
8 Y. Liang, Y. Li, H. Wang, J. Zhou, J. Wang, T. Regier and H. Dai, *Nat. Mater.*, 2011, **10**, 780–786.
9 M. R. Gao, J. Jiang and S. H. Yu, *Small*, 2012, **8**, 13–27.
10 J. P. Paraknowitsch and A. Thomas, *Energy Environ. Sci.*, 2013, **6**, 2839–2855.
11 H. J. Tang, H. J. Yin, J. Y. Wang, N. L. Yang, D. Wang and Z. Y. Tang, *Angew. Chem. Int. Ed.*, 2013, **52**, 5585–5589.
12 R. Liu, D. Wu, X. Feng and K. Müllen, *Angew. Chem. Int. Ed.*, 2010, **49**, 2565–2569.
13 Y. Zhi, N. Huagui, C. Xi'an, C. Xiaohua and H. Shaoming, *J. Power Sources*, 2013, **236**, 238–249.
14 S. Zhao, H. Yin, L. Du, L. He, K. Zhao, L. Chang, G. Yin, H. Zhao, S. Liu and Z. Tang, *ACS Nano*, 2014, **8**, 12660–12668.
15 S. Ni, Z. Li and J. Yang, *Nanoscale*, 2012, **4**, 1184–1189.
16 I.-Y. Jeon, D. Yu, S.-Y. Bae, H.-J. Choi, D. W. Chang, L. Dai and J.-B. Baek, *Chem. Mater.*, 2011, **23**, 3987–3992.
17 W. Wei, H. W. Liang, K. Parvez, X. D. Zhuang, X. L. Feng and K. Mullen, *Angew. Chem. Int. Ed.*, 2014, **53**, 1570–1574.
18 Z.-H. Sheng, L. Shao, J.-J. Chen, W.-J. Bao, F.-B. Wang and X.-H. Xia, *ACS Nano*, 2011, **5**, 4350–4358.
19 S. Chen, J. Bi, Y. Zhao, L. Yang, C. Zhang, Y. Ma, Q. Wu, X. Wang and Z. Hu, *Adv. Mater.*, 2012, **24**, 5593–5597.
20 D. Geng, Y. Chen, Y. Chen, Y. Li, R. Li, X. Sun, S. Ye and S. Knights, *Energy Environ. Sci.*, 2011, **4**, 760–764
21 Y. Kim, J. Ihm, E. Yoon and G.-D. Lee, *Phys. Rev. B*, 2011, **84**, 075445.
22 M. M. Ugeda, I. Brihuega, F. Hiebel, P. Mallet, J.-Y. Veuillen, J. M. Gómez-Rodríguez and F. Ynduráin, *Phys. Rev. B*, 2012, **85**, 121402.
23. J. C. Meyer, et al., Nano Lett. **2008**, 8, 3582.